Optics Letters

# Enhanced two-photon amplification in superconductor-semiconductor plasmonic waveguides

Nir Strugo,[1] Krishna Balasubramanian,[1,2] Dmitry Panna,[1] and Alex Hayat[1,*]

[1]Department of Electrical Engineering, Technion—Israeli Institute of Technology, Haifa 32000, Israel
[2]Department of Electrical Engineering, Indian Institute of Technology, Kanpur 208016, India
*Corresponding author: alex.hayat@technion.ac.il

Received 16 January 2020; accepted 26 February 2020; posted 4 March 2020 (Doc. ID 387928); published 31 March 2020

**We theoretically demonstrate significant enhancement of two-photon amplification by using a superconductor for both a Cooper-pair source and surface plasmon-polariton mode guiding. Cooper-pair-based gain active region restriction to the superconductor-semiconductor interface limits its potentially highly efficient two-photon gain process. Using the superconductor layer for a plasmonic waveguide structure allows strong photon confinement while reducing design and fabrication constraints. This results in three orders of magnitude enhancement of the superconducting two-photon gain (TPG) compared to superconductor-based dielectric waveguides. Moreover, a superconducting TPG produced by a plasmonic waveguide increases with carrier concentration, meeting practical device requirements. Our results pave the way for efficient two-photon amplification realization in nanoscale devices.** 

https://doi.org/10.1364/OL.387928

Stimulated two-photon emission (TPE) has been aimed for two-photon light sources since the days of the first laser demonstration [1,2] and has been useful in various fields of science and modern technologies. Stimulated TPE is being utilized in fields such as state squeezing in quantum optics [3], two-photon lasers [4–6], and optical pulse design—including ultrafast pulse compression [7], stable self mode-locked pulses [8], and giant pulse generation [9]. In semiconductors, an electrically pumped waveguide with a forward-biased PN-junction can be used to produce effective fully stimulated two-photon amplification, namely two-photon gain (TPG) [10,11]. Placing a superconductor layer on top of such a structure while using heavy doping allows the injection of Cooper-pairs (CP) into the semiconductor by the proximity effect [12]. The recombination of a CP with a pair of normal holes in the semiconductor PN-junction results in TPE [13]. Under the right input seed wavelength with merely picojoule-scale pulse energy, a strong CP-based superconducting TPG (STPG) can be achieved, comparable to the first-order process of one-photon gain [14]. An effective TPG process requires a large overlap between the waveguide transverse mode, the PN-junction active region where radiative recombination occurs, and the CP penetration profile. However, small CP penetration depth and restricted PN-junction active region width limit the CP-active-region (defined as the region dominated by Cooper-pair radiative recombination) to a thin layer close to the superconductor-semiconductor interface (Fig. 1). As a result, the efficiency of the STPG process is low in conventional dielectric waveguide structures due to the small overlap between the CP-active-region and the non-strongly confined waveguide transverse mode, located far from the superconductor interface, as illustrated in Fig. 1(a).

Here a significant enhancement of the STPG process is theoretically demonstrated in the optical wavelength range by using the superconductor layer as part of a plasmonic waveguide structure, supporting surface plasmon-polariton (SPP)

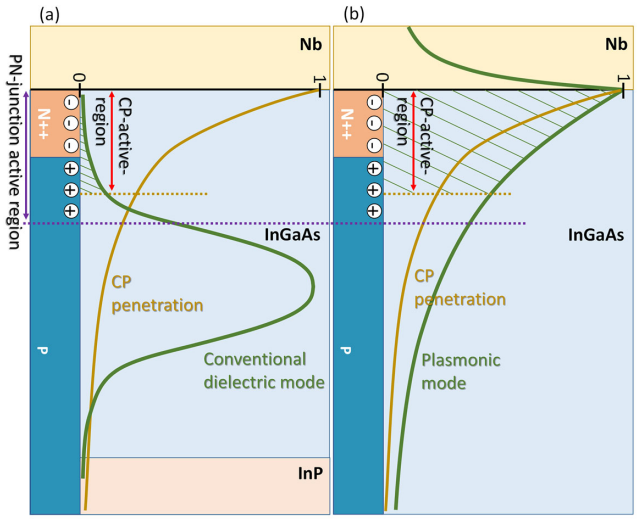


**Fig. 1.** Illustrated enhancement of transverse modal power confinement between a superconductor-based (a) conventional dielectric waveguide structure and (b) plasmonic waveguide structure. The modal power confinement (dashed area) is the overlap between the waveguide mode (green) and the CP-active-region depth (red), where the CP-active-region depth is the overlap between the PN-junction active region (purple) and the CP penetration (brown) depths. In this example, the latter sets the limit as it is shorter.

modes, in addition to being the Cooper-pair source. Our calculations show that the large overlap between the thin CP-active-region and the highly confined plasmonic modes, as illustrated in Fig. 1(b), provides three orders of magnitude increase to the modal STPG coefficient in comparison with the superconductor-based conventional dielectric waveguide structure. In addition, a dielectric waveguide structure has restrictions such as a refractive index profile and the use of thick layers comparable to the seed wavelength, required to support optical waveguiding. The use of a plasmonic waveguide structure eliminates these restrictions, allowing reduction of design and fabrication constraints. We further study the effects of various carrier concentration levels on the waveguide transverse modal power confinement in the CP-active-region ($\Gamma$) and the modal gain parameters. We show that TPG produced in a plasmonic waveguide increases with carrier concentration and hence meets practical device requirements.

A comparison was conducted between two superconductor-based structures that support STPG—a plasmonic waveguide and a conventional dielectric waveguide. We have designed our waveguide structures as a PN-junction stack of heavily doped N-type $In_{0.53}Ga_{0.47}As$ layer, with carrier concentration of $n > 10^{18}$ cm$^{-3}$ (to narrow the Schottky barrier width and thus improve CP injection efficiency) on top of a P-type bulk $In_{0.53}Ga_{0.47}As$. With a superconducting niobium (Nb) layer on top of the entire PN stack. The PN-junction location was designed to form the active region beginning from the superconductor interface, providing maximal overlap with the injected CP. To fully utilize the gain region, the conventional dielectric waveguide structure was designed to support a mode closer to the superconductor layer with the total InGaAs active layer thickness being 30% of the seed photon wavelength. In the plasmonic waveguide case, the SPP mode has a sub-wavelength confinement to the superconductor-semiconductor interface [15], with an evanescent field towards the PN stack. Hence, the overall InGaAs thickness was designed to exceed the theoretical CP-active-region depth. A femtosecond seed pulse was considered, allowing interaction with the Cooper-pair before superconducting suppression occurs due to the optical frequency photon energy—a process that takes several picoseconds and around 100 ps for the superconductivity to recover [16,17].

The CP-active-region is formed as a thin layer underneath the superconductor strip layer. Its depth, measured from the superconductor interface towards the semiconductor, is defined as the overlap between the CP penetration and PN-junction active region. To evaluate the effect of carrier concentration on the CP-active-region depth, we have calculated the depths of these components for carrier concentration levels in the range of $10^{16} - 10^{19}$ cm$^{-3}$. The CP penetration profile follows the CP pairing amplitude, $\Delta(x)$, which decays spatially [13]:

$$\Delta(x) \propto \Delta_0 \exp\left(-\frac{x}{\xi\,(n)}\right), \tag{1}$$

where $x$ is the distance from the superconductor-semiconductor interface, $n$ is the carrier concentration originated from doping, $\xi(n)$ is the CP coherence length, and $\Delta_0$ represents the superconducting gap. Hence, the CP penetration depth follows the CP coherence length which is proportional to $n^{\frac{1}{3}}$ [18]. The PN-junction active region depth is proportional to $n^{-\frac{1}{2}}$ [19]. As the depths of these two components have opposite trends, the CP-active-region depth dependence on carrier concentration is concave, with a maximum depth value of 60 nm for $n = 8 \times 10^{17}$ cm$^{-3}$. The CP penetration is the limiting factor for lower carrier concentration levels and the PN-junction active region for higher concentration levels.

We have calculated the plasmonic (based on SPP dispersion relation [20]) and conventional modes power confinement in the CP-active-region. Figure 2 depicts the compared waveguide structures and their mode overlap with the CP-active-region for carrier concentration of $n = 2 \times 10^{18}$ cm$^{-3}$. In this example, the highly confined SPP mode achieves ~45 times higher modal power confinement than in the conventional dielectric waveguide case. Modal power confinement results for a wide seed energy range and carrier concentration levels are presented in Fig. 3. The CP-active-region dependency on carrier concentration is witnessed in both waveguide structures, presenting a concave trend power confinement behavior with the same concentration level at the confinement maxima. The conventional dielectric waveguide, however, is prone to steeper dependence on carrier concentration due to the mode peak location being farther away from the CP-active-region. In addition, as the seed photon energy increases, the guided mode is more confined to the CP-active-region, and hence the power confinement increases in both waveguide structures. The calculated plasmonic mode power confinement values were at the range of 9–70%, much higher than those of the conventional counterpart, which were at the range of 0.04–2.4%. In the derivations, we considered doped $In_{0.53}Ga_{0.47}As$ with applied forward-biased voltage. The Nb refractive index was taken from Golovashkin *et al.* results at temperature of 4K [21].

To derive the transverse modal STPG coefficient $g_2 = g_2' I$, we start from the transverse intensity modal gain per propagation unit length, $g$, given by Ref. [10]:

$$\frac{dI}{dz} = g\,I = \left(g_1 + g_2' I\right) I, \tag{2}$$

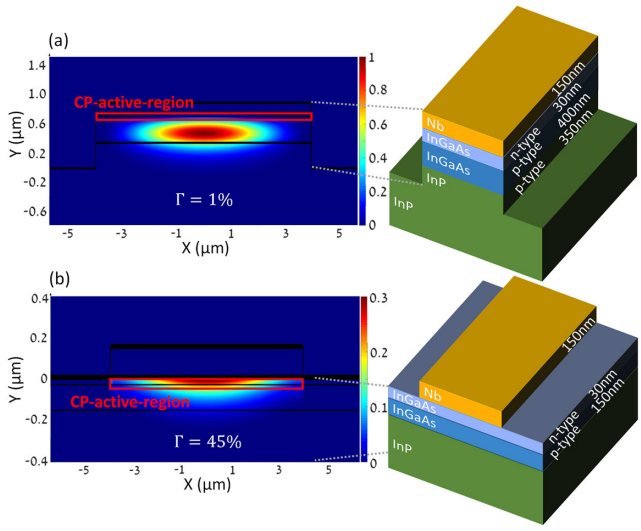


**Fig. 2.** (a) Dielectric and (b) plasmonic waveguide structures with their mode intensity cross sections for $n = 2 \times 10^{18}$ cm$^{-3}$ and 1.45 μm wavelength seed at 4 K. The CP-active-region is identical for both cases and marked as a red rectangle. (a) Left, conventional dielectric waveguide mode with modal power confinement of 1%. (b) Left, SPP mode with modal power confinement of 45%.

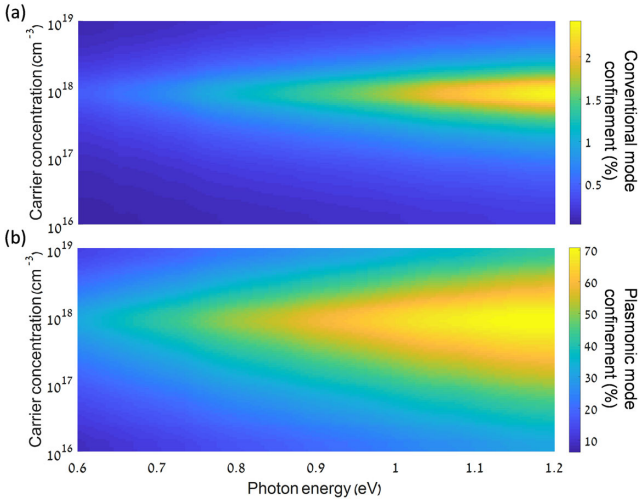


**Fig. 3.** Waveguide modal power confinement percentage in the CP-active-region as a function of the seed photon energy and carrier concentration level for (a) a conventional dielectric waveguide structure and (b) a plasmonic waveguide structure.

where $z$ is the mode propagation direction, $I(z)$ is the modal intensity, and $g_1$ is the transverse modal one-photon gain coefficient. We define $\gamma(x,y)=\gamma_1(x,y)+\gamma_2'(x,y)I$ as the transverse spatially dependent material gain, while $\gamma_1(x,y)$ and $\gamma_2'(x,y)$ represent the one-photon and superconducting TPG coefficients, respectively. Using $\gamma(x,y)$ and the mode electric field $\mathcal{E}(x,y,z)$, the transverse modal gain can be derived from Ref. [22]:

$$g=\frac{\iint \mathcal{E}^*(x,y,z)\,\gamma(x,y)\,\mathcal{E}(x,y,z)\,\mathrm{d}x\mathrm{d}y}{\iint |\mathcal{E}(x,y,z)|^2\mathrm{d}x\mathrm{d}y}. \tag{3}$$

The electric field according to its transverse and longitudinal components is $\mathcal{E}(x,y,z)=\mathcal{U}(x,y)\mathcal{E}_z(z)$, with normalized transverse component $\mathcal{U}(x,y)$. By neglecting the STPG contribution outside the CP-active-region cross section (A), the STPG coefficient is given by:

$$g_2=\frac{|\mathcal{E}_z(z)|^4\iint_A \gamma_2'(x,y)\,|\mathcal{U}(x,y)|^4\mathrm{d}x\mathrm{d}y}{|\mathcal{E}_z(z)|^2\iint_\infty |\mathcal{U}(x,y)|^2\mathrm{d}x\mathrm{d}y}, \tag{4}$$

and by using the intensity transverse and longitudinal components, defined as $I(x,y,z)=|\mathcal{E}(x,y,z)|^2=P(z)\sigma(x,y)$,

$$g_2=P(z)\iint_A \gamma_2'(x,y)\,\sigma^2(x,y)\,\mathrm{d}A. \tag{5}$$

Assuming a two-photon seed with two energies $E_{\mathrm{ph},1}$, $E_{\mathrm{ph},2}$ and temperature $T\to 0$, the spatially dependent CP-based STPG is given by Ref. [14]:

$$\gamma_2'(x,y)\propto |B|^4\left(\frac{\Delta(x)}{\Omega(x)}\right)^2\left[\frac{1}{\left(\left|\Delta_{E\mathrm{ph}1,2}\right|-\Omega(x)\right)^2}+\frac{1}{\left(\left|\Delta_{E\mathrm{ph}1,2}\right|+\Omega(x)\right)^2}\right], \tag{6}$$

where $B$ is the light-matter coupling energy with the quasi-particle, $\Delta_{E\mathrm{ph}1,2}$ the difference between the seed photon energies, $\Omega^2(x)=(E_{ph,1}+E_{\mathrm{ph},2}-2E_{fc})^2+4\Delta(x)^2$, and $E_{fc}$ is the conduction quasi-Fermi energy measured from the valence band edge $E_v$. For the Fermi-level calculations, we considered the InGaAs gap energy [23] and bandgap shrinkage [24] as a function of the evaluated temperature and carrier concentration levels. Free-carrier absorption effects [25] were taken into account in our carrier density integral calculation. Other $In_{0.53}Ga_{0.47}As$ parameters used were electron and hole effective masses of 0.054 and 0.463 [26], respectively, a dielectric constant of 13.89 F/m [27], and electron mobility of 4000 $cm^2/(Vs)$ [28].

The STPG coefficient was also calculated over a range of carrier concentration levels and seed energies for both the plasmonic and conventional dielectric waveguides, with the results presented in Fig. 4. The calculations were carried assuming a seed of two energies with matching detuning energy $\delta_E$, above and below the recombination energy from the Fermi level ($E_{\mathrm{ph}}=E_{fc}+\epsilon_p\pm\delta_E$), where $\epsilon_p$ represents a hole carrier energy below $E_v$ which we assume to be sufficiently small to neglect. For both waveguide structures, the typical TPE behavior of $1/E_{\mathrm{ph}}^2$ [29], derived from a second-order time-dependent perturbation theory, was witnessed along the photon energy axis, as shown in Fig. 4(d). A resonance peak around seed energy $E_{\mathrm{ph}}=E_{fc}\pm\Delta_0$ arises from the STPG resonance term [Eq. (6)] which corresponds to the CP quasi-particle density-of-states peak [30]. The colored columns in Figs. 4(a) and 4(b) represent the STPG resonance peak behavior per carrier concentration level. As higher concentration levels impose higher quasi Fermi

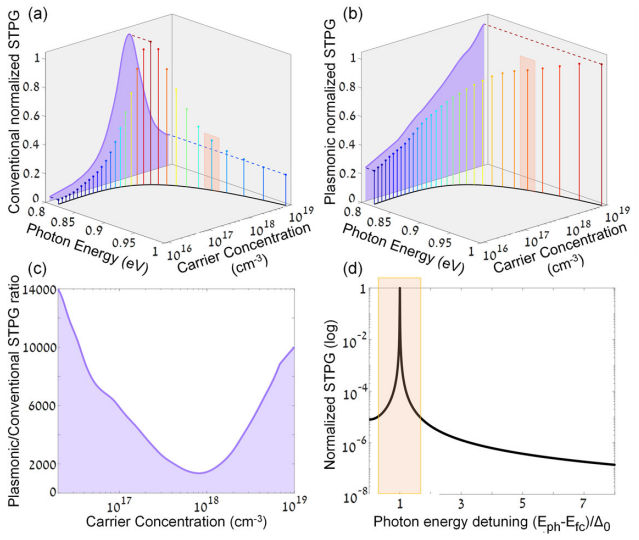


**Fig. 4.** Normalized STPG coefficient as a function of carrier concentration and seed photon energy for (a) a conventional dielectric waveguide structure and (b) a plasmonic waveguide structure. The colored columns represent the photon resonance energy at maximum STPG for a given carrier concentration level, and the purple projection presents the STPG magnitude trend. (c) STPG ratio between the plasmonic and the conventional dielectric waveguides as a function of carrier concentration level. (d) Normalized log-scale STPG as a function of the seed photon energy, detuned from the conduction-band quasi Fermi level ($E_{fc}$) and normalized by the superconducting gap energy for the $n=10^{17}$ $cm^{-3}$ case. It describes the behavior along the photon energy axis around the resonance peak for each colored column on subfigures (a) and (b) (as depicted by the orange square). The energy axis represents the higher energy photon of the two seed energies.

levels, the seed photon energy required for the STPG resonance increases. The STPG amplitude behavior is influenced by its dependence on the CP pairing amplitude ($\Delta^2$) and CP-active-region depth changes. As the carrier concentration level increases, so does the CP coherence length, and hence the CP pairing amplitude is larger throughout the CP-active-region. This increases the STPG for both waveguide structures along the carrier concentration levels, whereas the changes in the CP-active-region depth mainly affect the sparsely confined conventional dielectric waveguide, as previously shown. As a result, the STPG in a conventional dielectric waveguide structure is governed by the concave trend of the CP-active-region depth, with a maximum value at the same carrier concentration level, while in a plasmonic waveguide structure it rises with the carrier concentration. These behavior trends are depicted by the purple projections in Figs. 4(a) and 4(b). While most pronounced at the resonance seed energy, similar STPG behavior per carrier concentration was witnessed for other seed energies, equally spaced from the quasi Fermi level. An analysis of the STPG ratio between the plasmonic and conventional dielectric waveguides clearly shows that the plasmonic waveguide STPG is much stronger than its conventional dielectric counterpart throughout the entire evaluated carrier concentration and energy levels, as shown on Fig. 4(c). The plasmonic waveguide STPG is at least $\sim$1750 times stronger at $n = 8 \times 10^{17}$ cm$^{-3}$, where the STPG is maximal for the conventional dielectric waveguide structure, and up to $\sim$10,000 times stronger at $n = 10^{19}$ cm$^{-3}$. Although both the low and high carrier concentration regions exhibit high STPG ratio values, the higher concentration levels are required to maximize the STPG itself.

In conclusion, we have theoretically demonstrated that a superconductor-semiconductor plasmonic waveguide produces superior two-photon amplification, while reducing design and fabrication constraints. The plasmonic waveguide structure provides three orders of magnitude enhancement of the Cooper-pair-based STPG coefficient over the superconductor-based conventional dielectric waveguide structure, allowing a practical approach to achieve efficient TPG comparable to the one-photon gain process with merely picojoule-scale pulse energy. Our calculations show that higher carrier concentration levels increase the performance of the STPG achieved by a plasmonic waveguide over the conventional dielectric waveguide structure. Moreover, the use of a plasmonic waveguide with higher carrier concentration levels results in higher modal STPG coefficient. This trend meets the heavy doping requirement for effective Cooper-pair injection into the semiconductor. Although we chose to use $In_{0.53}Ga_{0.47}As$ as the semiconductor gain material, widely utilized in telecommunication, other compositions can be used in order to tune the gain wavelength and, as a result, the plasmonic mode propagation distance. Our results enable the realization of efficient two-photon amplification in nanoscale devices and offer opportunities in the fields of pulse design, nonlinear photonics, and quantum optics.

**Disclosures.** The authors declare no conflicts of interest.

## REFERENCES


1. P. P. Sorokin and N. Braslau, IBM J. Res. Dev. **8**, 177 (1964).
2. A. M. Prokhorov, Science **149**, 828 (1965).
3. M. O. Scully, K. Wodkiewicz, M. S. Zubairy, J. Bergou, N. Lu, and J. Meyer Ter Vehn, Phys. Rev. Lett. **60**, 1832 (1988).
4. H. P. Yuen, Phys. Rev. A **13**, 2226 (1976).
5. C. Z. Ning, Phys. Rev. Lett. **93**, 187403 (2004).
6. A. Hayat, P. Ginzburg, and M. Orenstein, Nat. Photonics **2**, 238 (2008).
7. A. Nevet, A. Hayat, and M. Orenstein, Opt. Lett. **35**, 3877 (2010).
8. D. R. Heatley, C. N. Ironside, and W. J. Firth, Opt. Lett. **18**, 628 (1993).
9. H. P. Yuen, Appl. Phys. Lett. **26**, 505 (1975).
10. A. Nevet, A. Hayat, and M. Orenstein, Phys. Rev. Lett. **104**, 207404 (2010).
11. C. N. Ironside, IEEE J. Quantum Electron. **28**, 842 (1992).
12. A. Kastalsky, L. H. Greene, J. B. Barner, and R. Bhat, Phys. Rev. Lett. **64**, 958 (1990).
13. Y. Asano, I. Suemune, H. Takayanagi, and E. Hanamura, Phys. Rev. Lett. **103** 187001 (2009).
14. R. Marjieh, E. Sabag, and A. Hayat, New J. Phys. **18**, 023019 (2016).
15. A. H. Majedi, IEEE Trans. Appl. Supercond. **19**, 907 (2009).
16. R. Singh and N. Zheludev, Nat. Photonics **8**, 679 (2014).
17. M. Beck, M. Klammer, S. Lang, P. Leiderer, V. V. Kabanov, G. N. Gol'Tsman, and J. Demsar, Phys. Rev. Lett. **107**, 177007 (2011).
18. H. Sasakura, S. Kuramitsu, Y. Hayashi, K. Tanaka, T. Akazaki, E. Hanamura, R. Inoue, H. Takayanagi, Y. Asano, C. Hermannstädter, H. Kumano, and I. Suemune, Phys. Rev. Lett. **107**, 157403 (2011).
19. R. F. Pierret, *Semiconductor Device Fundamentals* (Pearson Education India, 1996).
20. A. V. Zayats, I. I. Smolyaninov, and A. A. Maradudin, Phys. Rep. **408**, 131 (2005).
21. A. I. Golovashkin, I. E. Leksina, G. P. Motulevich, and A. A. Shubin, Phys. JETP **29**, 27 (1969).
22. L. A. Coldren, S. W. Corzine, and M. L. Mašanović, *Diode Lasers and Photonic Integrated Circuits* (Wiley, 2012).
23. S. Paul, J. B. Roy, and P. K. Basu, J. Appl. Phys. **69**, 827 (1991).
24. W. S. Cho, M. Luisier, D. Mohata, S. Datta, D. Pawlik, S. L. Rommel, and G. Klimeck, Appl. Phys. Lett. **100**, 063504 (2012).
25. B. R. Bennett, R. A. Soref, and J. A. Del Alamo, IEEE J. Quantum Electron. **26**, 113 (1990).
26. Q. X. Zhao, P. O. Holtz, B. Monemar, T. Lundström, J. Wallin, and G. Landgren, Phys. Rev. B **48**, 11890 (1993).
27. Y. A. Goldberg and N. M. Schmidt, *Handbook Series on Semiconductor Parameters* (1999), Vol. **2**.
28. T. P. Pearsall, *GaInAsP Alloy Semiconductors* (Wiley, 1982).
29. M. Göppert-Mayer, Ann. Phys. **401**, 273 (1931).
30. M. Tinkham, *Introduction to Superconductivity* (Courier, 2004).